Electromagnetically Coupled Coaxial Dipole Array Antenna

Hiroaki Miyashita, *Member, IEEE*, Hiroyuki Ohmine, *Member, IEEE*, Kazushi Nishizawa, *Member, IEEE*, Shigeru Makino, *Senior Member, IEEE*, and Shuji Urasaki, *Senior Member, IEEE*

***Abstract*—A new type of collinear antenna called electromagnetically coupled coaxial dipole array antenna is proposed. The antenna has an advantage of structural simplicity due to a novel use of an electromagnetically coupled feed structure for the radiating element. An analysis of the radiating element is presented and compared with experimental results. Fabrication and measurement of a prototype array antenna are also presented.**

***Index Terms*—Dipole arrays.**

I. Introduction

In this paper, a new type of collinear antenna is proposed that has an omnidirectional pattern in the horizontal plane. Fig. 1 shows the geometry of the antenna called electromagnetically coupled coaxial dipole array antenna. It has the electromagnetically coupled coaxial dipole (ECCD) as the radiating element, which is composed of a half-wavelength metallic circular pipe fed electromagnetically by an annular ring slot on the outer conductor of the feeding coaxial cable. The metallic circular pipes act as radiating dipoles and their collinear arrangement in the vertical direction with in-phase excitation gives an array performance.

There exist some kinds of collinear antennas. The coaxial collinear (COCO) antenna [1]–[4] employs a collinear arrangement of coaxial cables where the feeding structures are inverted in a half-wavelength step so as to produce in-phase excitations. Instead of using the coaxial cable, a printed COCO antenna with microstrip feed line is also reported [5]. An additional type is the coaxial dipole antenna (CDA) [6]. The radiating dipoles of CDA is fed by an annular ring slot, which extends radially from the outer conductor of the feeding coaxial cable. A modification of CDA is the bidirectional collinear antenna [7], which uses an arc parasitic plate attached near the radiating dipole of CDA.

ECCD array antenna, as proposed in this paper, is another modification of CDA, which has an advantage of structural simplicity due to a novel use of an electromagnetically coupled feed for CDA.

In Section II, a Wiener–Hopf analysis [8]–[11] is carried out for the TEM-mode reflection coefficient of a coaxial cable that has a semi-infinite outer conductor [12]–[14]. The analysis deals with an exact solution as well as a simple approximate formula that is valid if the radius of the coaxial cable is much smaller than the operating wavelength. In Section III, the methods due to Chen and Keller [15], and Lee and Mittra [16] are applied to derive the input admittance of the radiating element. In Section IV, an analysis of radiation pattern of ECCD is carried out with an integral equation formalism by using Green's functions of a perfectly conducting circular cylinder. In Section V, an equivalent circuit for ECCD array is described, and, finally, in Section VI, fabrication and measurement of a prototype array antenna are described.

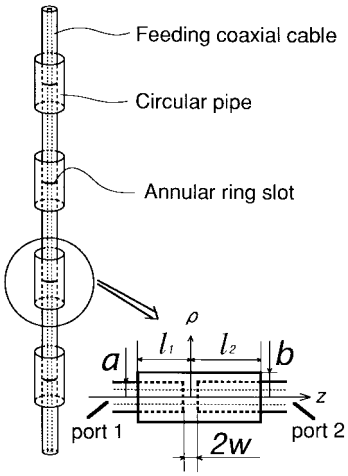

Fig. 1. The electromagnetically coupled coaxial dipole array antenna.

II. TEM-Mode Reflection Coefficient for a Semi-Infinite Coaxial Cable

In this section, a Wiener–Hopf analysis is carried out for the TEM-mode reflection coefficient of a semi-infinite coaxial cable, as shown in Fig. 2, when the TEM mode is incident from inside the cable. The structure is one of the canonical Wiener–Hopf geometries. Classic results for the TEM-mode incidence are given in [12] and the case of higher order modes incidence is treated in [14], where some approximate formulas are developed when the radius of the coaxial cable is much larger than the operating wavelength. In this paper, we derive an exact analytical expression as well as a simple approximate formula that is valid when the radius of the coaxial cable is much smaller than the operating wavelength. From now on, $e^{-i\omega t}$ dependence is assumed for the fields.

Manuscript received September 6, 1996; revised November 5, 1998.

H. Miyashita is with Kamakura Works, Mitsubishi Electric Corporation, Kamakura, Kanagawa, 247-8520 Japan. He is also with Radio Atmospheric Science Center, Kyoto University, Uji, Kyoto, 611-0011 Japan.

H. Ohmine, K. Nishizawa, S. Makino, and S. Urasaki are with the Information Technology R&D Center, Mitsubishi Electric Corporation, Kanagawa, 247-8501 Japan.

Publisher Item Identifier S 0018-926X(99)09395-3.

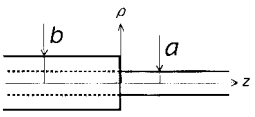

Fig. 2. Semi-infinite coaxial cable.

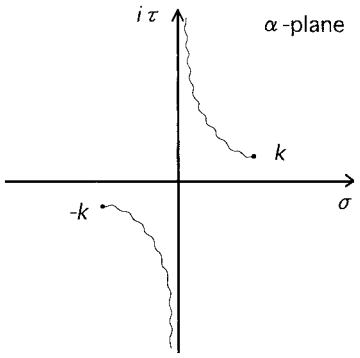

Fig. 3. Branch cut for the radial spectrum function γ in the α plane.

The problem has a rotational symmetry in the ϕ direction, and functional dependence of every physical quantity appears in the analysis is of the form $f(\rho, z)$. We define a Fourier transform pair of f with respect to z as follows:

$$F(\rho,\alpha) = \frac{1}{(2\pi)^{1/2}} \int_{-\infty}^{\infty} f(\rho,z) e^{i\alpha z}\, dz \tag{1}$$

$$f(\rho,z) = \frac{1}{(2\pi)^{1/2}} \int_{-\infty}^{\infty} F(\rho,\alpha) e^{-i\alpha z}\, d\alpha. \tag{2}$$

We assume that the propagation constant of the medium is $k = k_1 + ik_2 = \omega\sqrt{\mu\varepsilon}$, $k_1 \gg k_2 > 0$. k_2 will be put equal to zero after the analysis. The relation between α and the radial spectrum function γ are defined as follows (see Fig. 3):

$$\alpha = \sigma + i\tau, \quad \sigma, \tau : \text{real} \tag{3}$$

$$\gamma = (\alpha^2 - k^2)^{1/2} = -i\kappa = -i(k^2 - \alpha^2)^{1/2}. \tag{4}$$

For the geometry in Fig. 2, nonzero field components are expressed by using the vector potential $\mathbf{A} = \hat{z}\psi(\rho, z)$ as follows [9]:

$$E_z(\rho,z) = \frac{i}{\omega\varepsilon}\left(\frac{\partial^2}{\partial z^2} + k^2\right)\psi(\rho,z) \tag{5}$$

$$E_\rho(\rho,z) = \frac{i}{\omega\varepsilon}\frac{\partial^2}{\partial\rho\partial z}\psi(\rho,z) \tag{6}$$

$$H_\phi(\rho,z) = -\frac{\partial}{\partial\rho}\psi(\rho,z). \tag{7}$$

$\psi(\rho, z)$ satisfies the following wave equation:

$$\frac{1}{\rho}\frac{\partial}{\partial\rho}\left(\rho\frac{\partial\psi}{\partial\rho}\right) + \frac{\partial^2\psi}{\partial z^2} + k^2\psi = 0. \tag{8}$$

Let the incident TEM-mode current $I^i(z)$ have the following form in the region $(a \le \rho \le b)$:

$$I^i(z) = I_0 e^{ikz} = 2\pi\rho H_\phi^i(\rho,z), \quad I_0 = \text{const.} \tag{9}$$

The boundary conditions for the field components are given as follows:

$$E_z(a,z) = 0, \quad (-\infty < z < \infty) \tag{10}$$

$$E_z(b-,z) = E_z(b+,z) = 0 \quad (-\infty < z < 0) \tag{11}$$

$$E_z(b-,z) = E_z(b+,z) \equiv E_z(b,z) \quad (0 < z < \infty) \tag{12}$$

$$H_\phi(b+,z) - H_\phi(b-,z) = H_\phi^i(b,z), \quad (0 < z < \infty) \tag{13}$$

where $b+$ and $b-$ mean $b+\varepsilon$, $b-\varepsilon$, and $(\varepsilon \to +0)$, respectively, and this convention is applied throughout the paper. The edge condition for the end of the outer conductor is given as follows:

$$E_z(b,z) \sim z^{-1/2}, \quad (z \to 0) \tag{14}$$

$$H_\phi(b,z) \sim z^{+1/2}, \quad (z \to 0). \tag{15}$$

Let the Fourier transform of $\psi(\rho, z)$ with respect to z be $\Psi(\rho, \alpha)$, then (8) is equivalently expressed as follows:

$$\left[\frac{1}{\rho}\frac{\partial}{\partial\rho}\left(\rho\frac{\partial}{\partial\rho}\cdot\right) - \gamma^2\right]\Psi(\rho,\alpha) = 0, \quad |\tau| < k_2 \tag{16}$$

where γ is defined in (4). From now on, we put subscripts $+$ or $-$ on the function, which is regular in the upper half-plane $(\tau > -k_2)$ or regular in the lower half-plane $(\tau < k_2)$ in Fig. 3, respectively. In general, a Fourier transform $F(\alpha)$ of a function $f(z)$ is naturally decomposed into the sum of $F_+(\alpha)$ and $F_-(\alpha)$ [8]–[11]:

$$F(\alpha) = F_+(\alpha) + F_-(\alpha) \tag{17}$$

$$F_+(\alpha) = \frac{1}{(2\pi)^{1/2}} \int_0^{\infty} f(z) e^{i\alpha z}\, dz \tag{18}$$

$$F_-(\alpha) = \frac{1}{(2\pi)^{1/2}} \int_{-\infty}^{0} f(z) e^{i\alpha z}\, dz. \tag{19}$$

By using (5), (10), and the fact that the field decays as $\rho \to +\infty$, solutions for (16) are expressed as follows:

$$\Psi(\rho,\alpha) = \Psi_+(\rho,\alpha) + \Psi_-(\rho,\alpha) = A(\alpha)\frac{K_0(\gamma\rho)}{K_0(\gamma b)} \quad (\rho \ge b) \tag{20}$$

$$\Psi(\rho,\alpha) = B(\alpha)\frac{I_0(\gamma\rho)K_0(\gamma a) - K_0(\gamma\rho)I_0(\gamma a)}{I_0(\gamma b)K_0(\gamma a) - K_0(\gamma b)I_0(\gamma a)} \quad (a \le \rho \le b) \tag{21}$$

where, $A(\alpha)$ and $B(\alpha)$ are unknown functions. In the above formula, we have introduced normalization functions for later convenience. We define the Fourier transform of $E_z(\rho, z)$ and $H_\phi(\rho, z)$ with respect to z as $E(\rho, \alpha)$ and $H(\rho, \alpha)$. By using (5), (7), (20), and (21), we have the following relations:

$$E_+(b+,\alpha) + E_-(b+,\alpha) = \frac{\gamma^2}{i\omega\varepsilon}A(\alpha) \tag{22}$$

$$H_+(b+,\alpha) + H_-(b+,\alpha) = \frac{\gamma K_1(\gamma b)}{K_0(\gamma b)}A(\alpha) \tag{23}$$

$$E_+(b-,\alpha) + E_-(b-,\alpha) = \frac{\gamma^2}{i\omega\varepsilon}B(\alpha) \tag{24}$$

$$H_+(b-,\alpha)+H_-(b-,\alpha) = \gamma B(\alpha)\frac{I_1(\gamma b)K_0(\gamma a)+K_1(\gamma b)I_0(\gamma a)}{I_0(\gamma b)K_0(\gamma a)-K_0(\gamma b)I_0(\gamma a)}. \quad (25)$$

The boundary conditions (11)–(13) give the following:

$$E_-(b+,\alpha)=0 \quad (26)$$
$$E_-(b-,\alpha)=0 \quad (27)$$
$$E_+(b+,\alpha)=E_+(b-,\alpha)\equiv E_+(b,\alpha) \quad (28)$$

$$2\pi b\{H_+(b+,\alpha)-H_+(b-,\alpha)\} = \frac{1}{(2\pi)^{1/2}}\int_0^\infty I^i(z)e^{i\alpha z}\,dz = \frac{iI_0}{(2\pi)^{1/2}(\alpha+k)}. \quad (29)$$

The formulas (22), (24), and (26)–(28) give expressions of $A(\alpha)$ and $B(\alpha)$ as follows:

$$A(\alpha)=B(\alpha)=E_+(b,\alpha)\frac{i\omega\varepsilon}{\gamma^2}. \quad (30)$$

Next, we introduce an unknown function $J_-(\alpha)$ as follows:

$$2\pi b\{H_-(b+,\alpha)-H_-(b-,\alpha)\}=J_-(\alpha). \quad (31)$$

Subtracting (25) from (23) and using (29)–(31), we have the following Wiener–Hopf equation with respect to E_+ and J_-:

$$\frac{iI_0}{(2\pi)^{1/2}(\alpha+k)}+J_-(\alpha)+\frac{2\pi\omega\varepsilon E_+(b,\alpha)}{i\gamma^2L(\alpha)}=0 \quad (32)$$

$$L(\alpha)=\frac{K_0(\gamma b)}{K_0(\gamma a)}\{I_0(\gamma b)K_0(\gamma a)-K_0(\gamma b)I_0(\gamma a)\}. \quad (33)$$

$L(\alpha)$ can be factorized in a product form $L(\alpha)=L_+(\alpha)L_-(\alpha)$. The procedure is given in the Appendix. We rewrite (32) as follows:

$$\frac{iI_0}{(2\pi)^{1/2}(\alpha+k)}\{(\alpha-k)L_-(\alpha)+2kL_-(-k)\} + (\alpha-k)L_-(\alpha)J_-(\alpha) = \frac{2\pi\omega\varepsilon i}{(\alpha+k)L_+(\alpha)}E_+(b,\alpha)+\frac{2kI_0iL_-(-k)}{(2\pi)^{1/2}(\alpha+k)}. \quad (34)$$

The left-hand side and the right-hand side of the above formula are regular in $\tau<k_2$ and $\tau>-k_2$, respectively, in the α plane. Furthermore, they are both regular in $|\tau|<k_2$. Then the theorem of identity states that the both sides of (34) are identical to an integral function $P(\alpha)$ [8]–[11]. By using the edge condition and the results of the Appendix, the following relations are obtained in $|\tau|<k_2$ as $|\alpha|\to\infty$:

$$E_+(b,\alpha)\sim\alpha^{-1/2} \quad (35)$$
$$J_-(\alpha)\sim H_-(b,\alpha)\sim\alpha^{-3/2} \quad (36)$$
$$L_-(\alpha)\sim L_+(\alpha)\sim\alpha^{-1/2}. \quad (37)$$

By using the above properties, we see that the left-hand side of (34) decays as $\alpha^{-1/2}$ and the right-hand side decays as α^{-1} in $|\tau|<k_2$ when $|\alpha|\to\infty$. Then the Liouville's theorem states

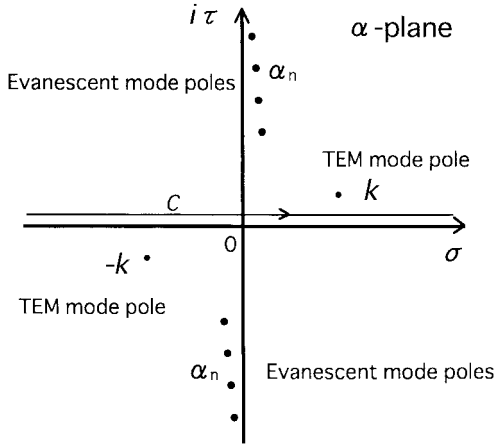

Fig. 4. The integration contour C and poles of the integrand of $U(\rho,z)$ in the α plane.

$P(\alpha)\equiv 0$ [8]–[11]. Thus, the solution of the Wiener–Hopf equation (32) is given as follows:

$$E_+(b,\alpha)=-\frac{\eta I_0}{(2\pi)^{1/2}\pi}L_+(\alpha)L_-(-k) \quad (38)$$

where, $\eta=\sqrt{\mu/\varepsilon}$. By using (25), (30), and (38), $H_\phi(\rho,z)$ is expressed in the region $(a\le\rho\le b)$ as follows:

$$H_\phi(\rho,z)=\frac{1}{(2\pi)^{1/2}}\int_{-\infty}^{\infty}H(\rho,\alpha)e^{-i\alpha z}\,d\alpha = \frac{kI_0i}{2\pi^2}L_-(-k)U(\rho,z) \quad (39)$$

$$U(\rho,z)=\int_C u(\rho,\alpha)e^{-i\alpha z}\,d\alpha \quad (40)$$

$$u(\rho,\alpha)=\frac{L_+(\alpha)}{\gamma}\cdot\frac{I_1(\gamma\rho)K_0(\gamma a)+K_1(\gamma\rho)I_0(\gamma a)}{I_0(\gamma b)K_0(\gamma a)-K_0(\gamma b)I_0(\gamma a)}.$$

If the radius of the coaxial cable is much smaller compared with the operating wavelength where only the TEM mode can propagate, the poles of the integrand of $U(\rho,z)$ are located in α plane, as shown in Fig. 4. In Fig. 4, the poles in the upper and lower half-planes correspond to the modes in the negative and positive z axis, respectively. The pole at $\alpha=k$ represents the reflected TEM mode from the discontinuous end of the coaxial cable. The pole at $\alpha=-k$ cancels the incident TEM mode in the positive z region.

By using the relations

$$I_0(\gamma b)K_0(\gamma a)-K_0(\gamma b)I_0(\gamma a)\to\ln\frac{b}{a},\quad(\gamma\to0) \quad (41)$$

$$I_1(\gamma\rho)K_0(\gamma a)+K_1(\gamma\rho)I_0(\gamma a)\sim\frac{1}{\gamma\rho},\quad(\gamma\to0) \quad (42)$$

the magnetic field $H_\phi^r(\rho,z)$ for the reflected TEM mode from the end of the coaxial cable is calculated by the residue of the pole at $\alpha=k$. Then the reflected current $I^r(z)$ is obtained as follows:

$$I^r(z)=2\pi aH_\phi^r(a,z) = -\frac{I_0}{\ln(b/a)}\{L_+(k)\}^2e^{-ikz} \quad (43)$$

The ratio of $I^r(z)$ and $I^i(z)$ gives the reflection coefficient $R(z)$ of the semi-infinite coaxial cable as follows:

$$R(z) = \frac{I^r(z)}{I^i(z)} = -\frac{1}{\ln(b/a)}\{L_+(k)\}^2 e^{-2ikz} \tag{44}$$

$$\begin{aligned} L_+(k) &= \left[\frac{\pi}{2}\{J_0(ka)N_0(kb) - N_0(ka)J_0(kb)\}\frac{H_0^{(1)}(kb)}{H_0^{(1)}(ka)}\right]^{\frac{1}{2}} \\ &\quad \cdot \exp\left[i\frac{k(b-a)}{\pi}\left\{1 + \ln 2 - \frac{\pi}{2} - C_e - \ln\frac{k(b-a)}{\pi i}\right\}\right] \\ &\quad \cdot \left[\prod_{n=1}^{\infty}\left(1 + \frac{k}{\alpha_n}\right)^{-k(b-a)/(n\pi i)}\right]\exp\{\xi(k,a,b)\} \end{aligned} \tag{45}$$

$$\xi(k,a,b) = q(k,b) - q(k,a) \tag{46}$$

$$q(k,x) = \int_0^{\infty} f(\omega,k,x)\,d\omega \tag{47}$$

$$f(\omega,k,x) = \frac{x}{\pi}\left[1 - \frac{2}{\pi\omega x}\cdot\frac{1}{\{J_0(\omega x)\}^2 + \{N_0(\omega x)\}^2}\right] \cdot \ln\left(1 + \frac{k}{\sqrt{k^2-\omega^2}}\right) \tag{48}$$

$$\sqrt{k^2-\omega^2} = i\sqrt{\omega^2-k^2} \tag{49}$$

where $C_e \simeq 0.5772$ is Euler's constant and α_n is defined as follows:

$$\begin{aligned} &I_0\big(\sqrt{\alpha_n^2-k^2}b\big)K_0\big(\sqrt{\alpha_n^2-k^2}a\big) \\ &\quad -K_0\big(\sqrt{\alpha_n^2-k^2}b\big)I_0\big(\sqrt{\alpha_n^2-k^2}a\big) = 0 \\ &\operatorname{Im}\alpha_n > 0, \quad \operatorname{Im}\alpha_n < \operatorname{Im}\alpha_{n+1}, \quad (n = 1,2,3,\cdots) \\ &\quad \alpha_n \sim \frac{in\pi}{b-a}, \quad (n \to \infty \text{ or } a,b \ll \lambda). \end{aligned} \tag{50}$$

Although (44) gives the exact solution, it has a disadvantage of practical applications because it contains infinite integrals as well as an infinite product. In general, a and b for ECCD are very small compared with the operating wavelength λ. In the following, we derive a simple approximate formula for R which is valid when $(0.001\lambda \le a,b \le 0.1\lambda)$.

The infinite integral given by (47) is evaluated numerically and an effort was made to find out an approximate numerical formula. It has been observed that in this case a polynomial of logarithmic variables improves the convergence with respect to the order of the series. The resultant expression of (47) in the domain $(0.001 \le x/\lambda \le 0.1)$ is as follows:

$$q(k,x) \equiv q(kx) \equiv Q(x/\lambda) \tag{51}$$

$$\begin{aligned} Q(x) \simeq &-0.160\,73 + 0.017\,312\ln x \\ &+ 0.009\,362\,8(\ln x)^2 + 0.000\,728\,49(\ln x)^3 \\ &+ i\{-0.023\,700 - 0.029\,142\ln x \\ &- 0.004\,772\,1(\ln x)^2 - 0.000\,215\,25(\ln x)^3\}. \end{aligned} \tag{52}$$

The above formula approximates the exact values within 3% errors. The part of infinite product is approximated as follows:

$$\prod_{n=1}^{\infty}\left(1 + \frac{k}{\alpha_n}\right)^{-k(b-a)/(i\pi n)}$$

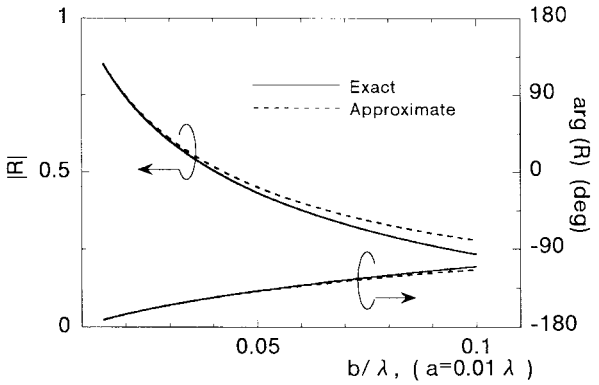

Fig. 5. Comparison between the exact formula (44) and the approximate formula (58).

$$\begin{aligned} &\simeq e^{-C_e k(b-a)/(i\pi)}\Big/\Gamma\left(1 + \frac{k(b-a)}{i\pi}\right) \\ &\simeq \exp\left[\frac{\{k(b-a)\}^2}{12}\right] \end{aligned} \tag{53}$$

where, the following formulas have been applied:

$$\alpha_n \simeq in\pi/(b-a) \tag{54}$$

$$\begin{aligned} \prod_{n=1}^{\infty}\left(1 + \frac{z}{an}\right)^{-z/(an)} &= \frac{e^{-C_e z/a}}{\Gamma(1+z/a)} \\ &\simeq \exp\left\{-\frac{\pi^2}{12}\left(\frac{z}{a}\right)^2\right\} \\ &\qquad (z/a \to 0). \end{aligned} \tag{55}$$

The error due to the approximation of α_n given in (54) in the domain $(0.001\lambda \le a,b \le 0.1\lambda)$ is within 10%. The remaining parts of (45) are approximated as follows:

$$\frac{\pi}{2}\{J_0(ka)N_0(kb) - N_0(ka)J_0(kb)\} \simeq \ln\frac{b}{a} \tag{56}$$

$$\frac{H_0^{(1)}(kb)}{H_0^{(1)}(ka)} \simeq \frac{\ln(kb/2) + C_e - i\pi/2}{\ln(ka/2) + C_e - i\pi/2}. \tag{57}$$

The final expression of $R(z)$ is given as follows:

$$R(z) \simeq -\frac{\ln(kb/2) + C_e - i\pi/2}{\ln(ka/2) + C_e - i\pi/2}\exp\{2(M - ikz)\} \tag{58}$$

$$\begin{aligned} M = &Q\left(\frac{b}{\lambda}\right) - Q\left(\frac{a}{\lambda}\right) + \frac{\{k(b-a)\}^2}{12} \\ &+ \frac{k(b-a)i}{\pi}\left\{1 + \ln 2 - \frac{\pi}{2} - C_e - \ln\frac{k(b-a)}{\pi i}\right\}. \end{aligned} \tag{59}$$

To see the validity of (58), a comparison is plotted in Fig. 5 between approximated values calculated by (58) and the exact values in the case of $a = 0.01\lambda$ and $0.015\lambda \le b \le 0.1\lambda$. The correspondence between them is appropriate for practical applications.

III. Input Admittance

In this section, the TEM-mode reflection coefficient for the semi-infinite coaxial cable is applied to an analysis of the input admittance of ECCD in Fig. 1. From now on we write

$R = R(0)$ in (58). We will derive an approximate form of the current distribution $I(z)$ on $\rho = a$ by the methods due to Chen and Keller [15] and Lee and Mittra [16]. In this case, we treat the region between the circular pipe and the feeding coaxial cable in Fig. 1 as a cavity, where TEM mode is the only propagation mode and the effect of end discontinuities is contained in R. We define $I_{\rm inf}(z)$ as a current on $\rho = a$, which is excited by the annular ring slot when the discontinuities of the coaxial line are absent. We also define $I_{\rm cav}(z)$ as currents due to multiple reflections between the ends of the cavity when the TEM-mode current in $I_{\rm inf}(z)$ is incident. $I_{\rm cav}(z)$ are identified as a Neumann series, which can be summed up in a closed form (for the details, see the derivation of [16, eq. (5.2)]). $I(z)$ is approximately calculated by superposition of $I_{\rm inf}(z)$ and $I_{\rm cav}(z)$ as follows:

$$I(z) \simeq I_{\rm inf}(z) + I_{\rm cav}(z) \tag{60}$$

$$I_{\rm inf}(z) = I_0 U(z) + I_{\rm np}(z) \tag{61}$$

$$\begin{aligned} I_{\rm cav}(z) &= I_0 \frac{U(l_1) + RU(l_2)U(l_1+l_2)}{1 - R^2\{U(l_1+l_2)\}^2} RU(z-l_1) \\ &\quad + I_0 \frac{U(l_2) + RU(l_1)U(l_1+l_2)}{1 - R^2\{U(l_1+l_2)\}^2} RU(z+l_2) \end{aligned} \tag{62}$$

$$U(z) = e^{ik|z|} \tag{63}$$

where the term $I_0 U(z)$ and $I_{\rm np}(z)$ in (61) correspond to the currents due to TEM mode and nonpropagating modes, respectively. If the annular ring slot in Fig. 1 is excited by a voltage Δv, the input admittance Y_{11} of ECCD is given as follows:

$$Y_{11} = \frac{I(w) + I(-w)}{2\Delta v} \tag{64}$$

$$\simeq Y_{\rm inf} + Y_{\rm cav} \tag{65}$$

$$Y_{\rm inf} = \frac{I_{\rm inf}(w) + I_{\rm inf}(-w)}{2\Delta v} \tag{66}$$

$$Y_{\rm cav} = \frac{I_{\rm cav}(w) + I_{\rm cav}(-w)}{2\Delta v}. \tag{67}$$

First, we will calculate $Y_{\rm inf}$. We assume that the width $2w$ of the annular ring slot is much smaller compared with λ, and it can be modeled by the following uniform magnetic current M_ϕ:

$$M_\phi(\rho, z) = \begin{cases} -\{\Delta v/(2w)\}\delta(\rho - a), & (|z| < w) \\ 0, & (|z| \geq w). \end{cases} \tag{68}$$

The only nonzero component of the magnetic field inside the coaxial cable is $H_\phi(\rho, z)$. We define the Green's function G with respect to M_ϕ as follows:

$$H_\phi(\rho, z) = i\omega\varepsilon \int_{-w}^{w} dz' \int_a^b \rho' d\rho'\, G(\rho, z \mid \rho', z') M_\phi(\rho', z') \tag{69}$$

$$\frac{\partial}{\partial \rho}\left\{\frac{1}{\rho}\frac{\partial}{\partial \rho}(\rho G)\right\} + \frac{\partial^2 G}{\partial z^2} + k^2 G = -\frac{\delta(\rho - \rho')}{\rho'}\delta(z - z'). \tag{70}$$

G can be constructed as follows:

$$G(\rho, z \mid \rho', z') = -\frac{e^{ik|z-z'|}}{2ik\rho\rho' \ln(b/a)} + \frac{1}{2}\sum_{n=1}^{\infty} \frac{P_n(\rho)P_n(\rho')}{\lambda_n F_n} e^{-\lambda_n |z-z'|}, \tag{71}$$

$$P_n(\rho) = J_1(p_n\rho)N_0(p_n a) - N_1(p_n\rho)J_0(p_n a) \tag{72}$$

$$\lambda_n = \sqrt{p_n^2 - k^2}, \quad \partial\{\rho P_n(\rho)\}/\partial\rho|_{\rho=b} = 0 \tag{73}$$

$$F_n = \frac{2}{\pi^2 p_n^2}\left[\left\{\frac{J_0(p_n a)}{J_0(p_n b)}\right\}^2 - 1\right]. \tag{74}$$

By using (68), (69), and (71), $I_{\rm inf}(z)$ is calculated as follows:

$$I_{\rm inf}(z) = 2\pi a H_\phi(a, z) \tag{75}$$

$$\begin{aligned} &= \frac{Y_0}{2}\Delta v \cdot \frac{\sin(kw)}{kw} U(z) \\ &\quad - \frac{i\pi k}{\eta w}\Delta v \sum_{n=1}^{\infty} \frac{1 - e^{-2\lambda_n w}}{\lambda_n^2}\left[\left\{\frac{J_0(p_n a)}{J_0(p_n b)}\right\}^2 - 1\right]^{-1} \\ &\simeq \frac{Y_0}{2}\Delta v \cdot U(z) \\ &\quad - \frac{i\pi k}{\eta w}\Delta v \sum_{n=1}^{\infty} \frac{1 - e^{-2\lambda_n w}}{\lambda_n^2}\left[\left\{\frac{J_0(p_n a)}{J_0(p_n b)}\right\}^2 - 1\right]^{-1} \end{aligned} \tag{76}$$

$$Y_0 = \frac{2\pi}{\eta \ln(b/a)}. \tag{77}$$

where (76) is obtained by assuming $kw \ll 1$. The first term and the last summation part in (76) are identified with $I_0 U(z)$ and $I_{\rm np}(z)$ in (61), respectively. By comparing the coefficients of $U(z)$ in the first terms in (61) and (76), we have the following relation:

$$I_0 = \frac{Y_0}{2}\Delta v. \tag{78}$$

$Y_{\rm inf}$ is obtained by (66) and (76) as follows:

$$Y_{\rm inf} \simeq \frac{Y_0}{2} - \frac{i\pi k}{\eta w}\sum_{n=1}^{\infty} \frac{1 - e^{-2\lambda_n w}}{\lambda_n^2}\left[\left\{\frac{J_0(p_n a)}{J_0(p_n b)}\right\}^2 - 1\right]^{-1} \tag{79}$$

where the approximation $U(\pm w) = e^{ik|w|} \simeq 1$ is made like in (76). $Y_{\rm cav}$ is readily obtained by (62), (67), and (78) as follows:

$$Y_{\rm cav} \simeq \frac{Y_0}{2} R \frac{\{U(l_1)\}^2 + \{U(l_2)\}^2 + 2R\{U(l_1+l_2)\}^2}{1 - R^2\{U(l_1+l_2)\}^2} \tag{80}$$

where the approximations $U(\pm w - l_1) \simeq U(l_1)$ and $U(\pm w + l_2) \simeq U(l_2)$ are made. By using (63), (65), (79), and (80), we finally obtain Y_{11} as follows:

$$\begin{aligned} Y_{11} &\simeq \frac{Y_0}{2} \cdot \frac{(1 + Re^{2ikl_1})(1 + Re^{2ikl_2})}{1 - R^2 e^{2ik(l_1+l_2)}} \\ &\quad - \frac{i\pi k}{\eta w}\sum_{n=1}^{\infty} \frac{1 - e^{-2\lambda_n w}}{\lambda_n^2}\left[\left\{\frac{J_0(p_n a)}{J_0(p_n b)}\right\}^2 - 1\right]^{-1}. \end{aligned} \tag{81}$$

In the case of $l_1 = l_2 = l$, (81) becomes

$$Y_{11}(l_1 = l_2 = l) \simeq \frac{Y_0}{2} \cdot \frac{1 + Re^{2ikl}}{1 - Re^{2ikl}} - \frac{i\pi k}{\eta w} \sum_{n=1}^{\infty} \frac{1 - e^{-2\lambda_n w}}{\lambda_n^2} \times \left[\left\{ \frac{J_0(p_n a)}{J_0(p_n b)} \right\}^2 - 1 \right]^{-1}. \quad (82)$$

When $R = 0$, the first term in (82) reduces to $Y_0/2$, which represents the admittance in the case of two coaxial lines connected and fed at the center. If we put $R = -1$ and $l = 1/4\lambda$ in (82), then $Y_{11} = \infty$, i.e., when each end of the coaxial cable is open-circuited and the location of the annular ring slot is a quarter wavelength away from the ends, the annular ring slot is short-circuited, which meets the physical inspection.

To verify the applicability of the derived formula, measurements were carried out. S parameters S_{11} and S_{21} were measured for the two ports 1 and 2 in Fig. 1 of the feeding coaxial cable with characteristic impedance Z_f. An equivalent circuit for the geometry consists of a transmission line with characteristic impedance Z_f loaded with input impedance Z_{11} of ECCD and Z_f in series. S_{11} and S_{21} are calculated as follows:

$$S_{11} = \frac{Z_{11}}{Z_{11} + 2Z_f} \quad (83)$$

$$S_{21} = \frac{2Z_f}{Z_{11} + 2Z_f} \quad (84)$$

$$Z_{11} = 1/Y_{11}. \quad (85)$$

Fig. 6 shows comparisons between the measured and calculated values. The parameters are $l_1 = l_2 = 0.21\lambda_{f0}$, $a = 0.0092\lambda_{f0}$, $b = 0.023\lambda_{f0}$, $w = 0.0041\lambda_{f0}$, and $Z_f = 50\ \Omega$, where λ_{f0} corresponds to the free-space wavelength at the frequency f_0.

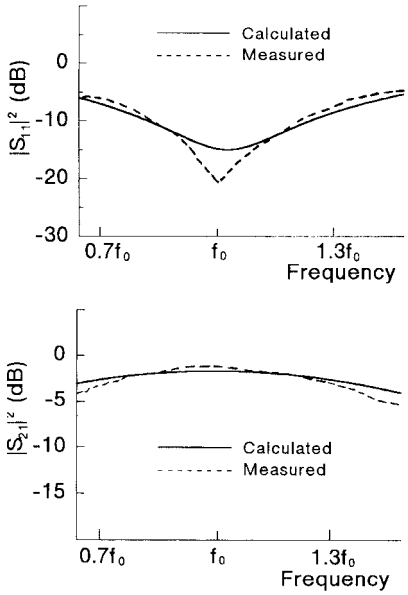

Fig. 6. Comparison between calculated and measured values for S_{11} and S_{21} of ECCD in Fig. 1, where $l_1 = l_2 = 0.21\lambda_{f0}$, $a = 0.0092\lambda_{f0}$, $b = 0.023\lambda_{f0}$, $w = 0.0041\lambda_{f0}$, and $Z_f = 50\ \Omega$.

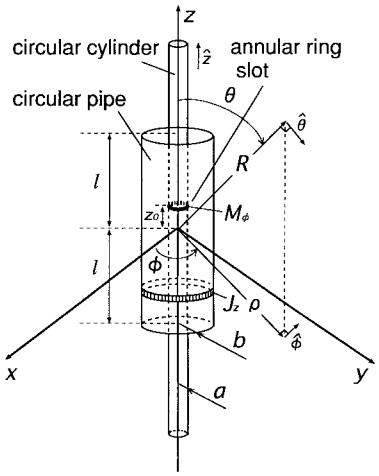

Fig. 7. Geometry of ECCD and rotationally symmetric electric and magnetic currents on a perfectly conducting infinite circular cylinder.

IV. Radiation Patterns

In this section, the radiation pattern of ECCD is analyzed. We model the circular pipe and the annular ring slot in ECCD as rotationally symmetric electric and magnetic currents, respectively, which are located above a perfectly conducting infinite circular cylinder of radius a, as shown in Fig. 7. Fields of the currents are expressed through Green's functions of the circular cylinder. The current distribution of the circular pipe is determined by an integral equation with respect to the electric field boundary condition on the surface of the pipe, then the radiation pattern is obtained.

The nonzero fields $E_z^{(e)}(\rho, z), E_\rho^{(e)}(\rho, z)$ and $H_\phi^{(e)}(\rho, z)$ of the $\hat{z}$-directed electric current $J_z(z')$ at the radius b are given by (5)–(7) with the vector potential $\psi(\rho, z)$ replaced by $A_z(\rho, z)$, which is calculated by the Green's function of the infinite circular cylinder [17] as follows:

$$A_z(\rho, z) = \int_{-l}^{l} dz'\, G^{(e)}(\rho, z \mid b, z') J_z(z') \quad (86)$$

$$G^{(e)}(\rho, z \mid b, z') = \frac{ib}{4} \int_{-\infty}^{\infty} d\alpha\, e^{i\alpha|z-z'|} \frac{H_0^{(1)}(\kappa\rho_>)}{H_0^{(1)}(\kappa a)} \cdot \left\{ J_0(\kappa\rho_<) H_0^{(1)}(\kappa a) - H_0^{(1)}(\kappa\rho_<) J_0(\kappa a) \right\} \quad (87)$$

where $\rho_>$ and $\rho_<$ represent, respectively, the larger and the smaller values of ρ and b, and κ is given in (4).

The nonzero fields of the $\hat{\phi}$-directed magnetic current $M_\phi(z')$ on the surface of the circular cylinder are given as follows [17]:

$$E_\rho^{(m)}(\rho, z) = \frac{1}{i\omega\varepsilon} \frac{\partial H_\phi^{(m)}}{\partial z} \quad (88)$$

$$E_z^{(m)}(\rho, z) = \frac{i}{\omega\varepsilon} \frac{1}{\rho} \frac{\partial}{\partial \rho} \left(\rho H_\phi^{(m)} \right) \quad (89)$$

$$H_\phi^{(m)}(\rho,z)=i\omega\varepsilon\int_{-w}^{w}dz'\,G^{(m)}(\rho,z\mid a,z')M_\phi(z') \tag{90}$$

$$G^{(m)}(\rho,z\mid a,z')=-\frac{1}{2\pi}\int_{-\infty}^{\infty}d\alpha\,e^{i\alpha|z-z'|}\frac{1}{\kappa}\frac{H_1^{(1)}(\kappa\rho)}{H_0^{(1)}(\kappa a)}. \tag{91}$$

If we treat M_ϕ as a known source, which gives an incident wave of the scattering problem, the following integral equation for J_z is obtained by the electric field boundary condition on the surface of the circular pipe

$$E_z^{(m)}(b,z)+E_z^{(e)}(b,z)=0,\quad(|z|\le l). \tag{92}$$

We will use Galerkin's method to solve the above integral equation. We expand $J_z(z)$ with a class of expansion functions $\Psi_n(z),(n=1,2,3,\cdots)$ as follows:

$$J_z(z)=\sum_{n=1}^{\infty}X_n\Psi_n(z) \tag{93}$$

$$\Psi_n(z)=\frac{1}{2l}\sin\Big\{\frac{n\pi}{2l}(z+l)\Big\} \tag{94}$$

where X_n, $(n=1,2,3,\cdots)$ are unknown coefficients to be determined. The integral equation (92) is equivalent to the following form in Galerkin's sense:

$$\int_{-l}^{l}dz\,\Psi_n(z)\big\{E_z^{(m)}(b,z)+E_z^{(e)}(b,z)\big\}=0 \qquad (n=1,2,3,\cdots). \tag{95}$$

After some calculations, by assuming $M_\phi(z)=M_0\delta(z-z_0)$ for simplicity, (95) reduces to the following simultaneous linear equations with respect to X_n

$$\sum_{n=1}^{\infty}A_{mn}X_n=P_m \tag{96}$$

$$A_{mn}=-\frac{\eta b}{2k}\int_0^{\infty}d\alpha\,B_{mn}(\alpha)\kappa^2\frac{H_0^{(1)}(\kappa b)}{H_0^{(1)}(\kappa a)}\cdot\big\{J_0(\kappa b)H_0^{(1)}(\kappa a)-H_0^{(1)}(\kappa b)J_0(\kappa a)\big\} \tag{97}$$

$$B_{mn}(\alpha)=C_m(\alpha)C_n(\alpha)+S_m(\alpha)S_n(\alpha) \tag{98}$$

$$P_m=-\frac{M_0}{\pi}\int_0^{\infty}d\alpha\,\frac{H_0^{(1)}(\kappa b)}{H_0^{(1)}(\kappa a)}\cdot\{C_m(\alpha)\cos(\alpha z_0)+S_m(\alpha)\sin(\alpha z_0)\} \tag{99}$$

$$C_n(\alpha)=\int_{-l}^{l}dz\,\Psi(z)\cos(\alpha z) \tag{100}$$

$$=\frac{n\pi\cos(\alpha l)}{(2\alpha l)^2-(n\pi)^2}\{(-1)^n-1\} \tag{101}$$

$$S_n(\alpha)=\int_{-l}^{l}dz\,\Psi(z)\sin(\alpha z) \tag{102}$$

$$=\frac{n\pi\sin(\alpha l)}{(2\alpha l)^2-(n\pi)^2}\{(-1)^n+1\}. \tag{103}$$

An approximate solution is obtained by replacing the summation in (96) by finite N terms and a matrix inversion. Now we calculate the radiation pattern of the current distribution. We will neglect contribution of M_ϕ for the radiation pattern by assuming that the dimension of the annular ring slot is much smaller compared with the circular pipe. The magnetic field $H_\phi^{(e)}$ of J_z is calculated by (7) and (86) as follows:

$$H_\phi^{(e)}(\rho,z)=\int_{-l}^{l}dz'\,G_H^{(e)}(\rho,z\mid b,z')J_z(z') \tag{104}$$

$$G_H^{(e)}(\rho,z\mid b,z')=-\frac{\partial}{\partial\rho}G^{(e)}(\rho,z\mid b,z') \tag{105}$$

$$=\frac{ib}{4}\int_{-\infty}^{\infty}d\alpha\,\kappa e^{i\alpha|z-z'|}\frac{H_1^{(1)}(\kappa\rho)}{H_0^{(1)}(\kappa a)}\cdot\big\{J_0(\kappa b)H_0^{(1)}(\kappa a)-H_0^{(1)}(\kappa b)J_0(\kappa a)\big\}\qquad(\rho\ge b). \tag{106}$$

In the far-field region, an asymptotic approximation can be employed for the integral in (106) with the aid of the following formula [17]:

$$\int_{-\infty}^{\infty}d\alpha\,F(\alpha,\kappa)H_n^{(1)}(\kappa\rho)e^{i\alpha|z|}\sim F(k\cos\theta,k\sin\theta)\frac{2}{R}e^{ikR-i(n+1)\pi/2} \tag{107}$$

$$z=R\cos\theta \tag{108}$$

$$\rho=R\sin\theta \tag{109}$$

$$R=\sqrt{\rho^2+z^2}. \tag{110}$$

The final expression of the far-field is given as follows:

$$E_\theta^{(e)}\simeq\eta H_\phi^{(e)} \tag{111}$$

$$\simeq\frac{e^{ikR}}{R}\cdot\frac{\eta kb\sin\theta}{2iH_0^{(1)}(ka\sin\theta)}\big\{J_0(kb\sin\theta)H_0^{(1)}(ka\sin\theta)-H_0^{(1)}(kb\sin\theta)J_0(ka\sin\theta)\big\}\sum_{n=1}^{N}X_nD_n(k\cos\theta) \tag{112}$$

$$D_n(\alpha)=\int_{-l}^{l}dz\,\Psi_n(z)e^{-i\alpha z} \tag{113}$$

$$=\frac{n\pi}{(2\alpha l)^2-(n\pi)^2}\{(-1)^ne^{-i\alpha l}-e^{i\alpha l}\}. \tag{114}$$

Fig. 8 shows the calculated and measured radiation patterns of ECCD in Fig. 7, where the parameters are the same as those in Fig. 6 in the previous section with $l=l_1=l_2$ and $z_0=0$.

V. Array Performance

ECCD array antenna with n radiating elements can be analyzed by an equivalent circuit for collinear antennas [18], [19] shown in Fig. 9. The feeding point of the array is located at the distance d_0 measured from the first radiating element and the end of the feeding coaxial cable, which is located at the distance d_n from the last radiating element, is terminated with

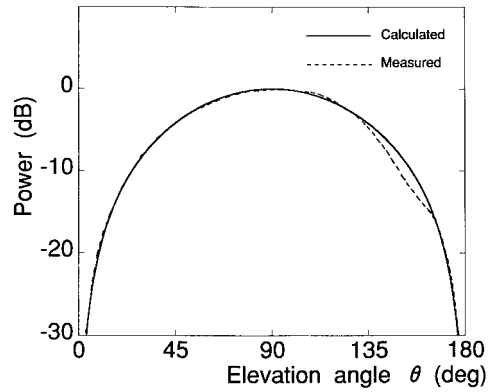

Fig. 8. Calculated and measured radiation pattern of ECCD, where the parameters are the same as those in Fig. 6.

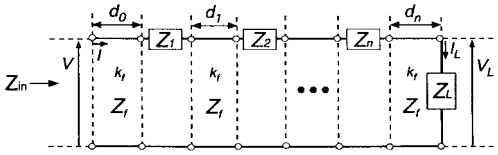

Fig. 9. Equivalent circuit for ECCD array antenna.

a load of impedance Z_L. d_m, $(m = 1, 2, \cdots, n-1)$ represent the spacings between mth and $m+1$th radiating elements. k_f and Z_f represent the propagation constant and the characteristic impedance of the feeding coaxial cable, respectively. Z_m, $(m = 1, 2, \cdots, n)$ represent the self impedances of mth radiating element which are calculated as follows:

$$Z_m = 1/Y_m \tag{115}$$

where Y_m stands for the self admittance of mth radiating element calculated by (81).

The input impedance Z_{in} of the array antenna is calculated by using the F matrices F_m^Z, F_m, $(m = 1, 2, \cdots, n)$ of the equivalent circuit as follows:

$$Z_{\text{in}} = \frac{V}{I} \tag{116}$$

$$\begin{pmatrix} V \\ I \end{pmatrix} = F_0 F_1^Z F_1 F_2^Z F_2 \cdots F_{n-1} F_n^Z F_n \begin{pmatrix} V_L \\ I_L \end{pmatrix} \tag{117}$$

$$V_L = Z_L I_L \tag{118}$$

$$F_m^Z = \begin{pmatrix} 1 & Z_m \\ 0 & 1 \end{pmatrix} \tag{119}$$

$$F_m = \begin{pmatrix} \cos\theta_m & -iZ_f \sin\theta_m \\ (-i/Z_f)\sin\theta_m & \cos\theta_m \end{pmatrix} \tag{120}$$

$$\theta_m = k_f d_m \tag{121}$$

where V, I and V_L, I_L represent the voltage and current at the feeding port and those at the termination, respectively, F_m^Z represents the F matrix of the serial impedance Z_m, and the effect of length d_m of the feeding coaxial cable is contained in F_m. It is noted that (118) is sufficient to determine (116) because $Z_{\text{in}}(V_L, I_L)$ in (116) depends only on the ratio of V_L and I_L. The voltage V_m and current I_m seen from the feed side at the mth radiating element are given as follows:

$$\begin{pmatrix} V_m \\ I_m \end{pmatrix} = F_m^Z F_m F_{m+1}^Z F_{m+1} \cdots F_{n-1} F_n^Z F_n \begin{pmatrix} V_L \\ I_L \end{pmatrix} \tag{122}$$

where $\Delta v_m = I_m Z_m$, $(m = 1, 2, \cdots, n)$ give the array excitation distributions.

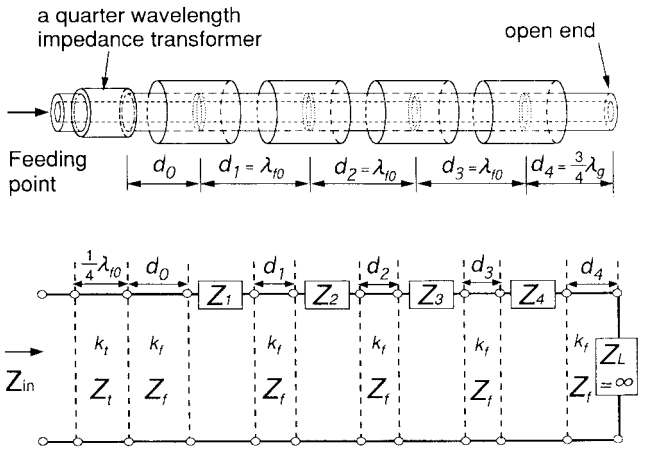

Fig. 10. Geometry and equivalent circuit of a prototype four-element ECCD array antenna, where the parameters of radiating elements are the same as those in Fig. 6, $\varepsilon_r = 2$ inside the feeding coaxial cable except in the quarter wavelength impedance transformer, where $\varepsilon_r = 1$, the inner and outer radii of the transformer, are $0.0026\lambda_{f0}$ and $0.010\lambda_{f0}$, respectively, and $d_0 = 0.44\lambda_g$.

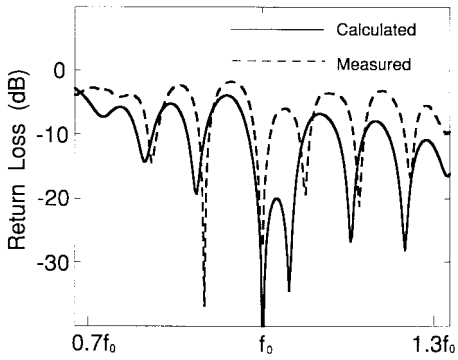

Fig. 11. Return loss (power) of ECCD array antenna in Fig. 10. The antenna is designed to be matched at f_0.

VI. Fabrication and Measurements

A four-element array antenna as shown in Fig. 10 was fabricated. The antenna was designed to have a uniform aperture field distribution. The parameters of the radiating elements are all identical to those of Figs. 6 and 8 in the previous sections. The inner and outer radii of the feeding coaxial cable are $0.0026\lambda_{f0}$ and $0.0085\lambda_{f0}$, respectively. The cable is filled with dielectric material of dielectric constant $\varepsilon_r = 2.0$. The spacings d_1, d_2, and d_3 between the radiating elements are all identical to $0.71\lambda_{f0}$, which corresponds to $1\lambda_g$ where $\lambda_g = \lambda_{f0}/\sqrt{\varepsilon_r}$. The feeding coaxial cable is

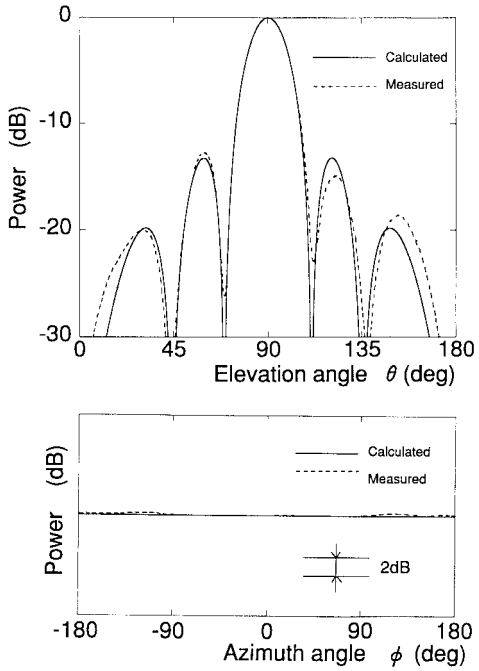

Fig. 12. Radiation characteristics of the four-element ECCD array antenna in Fig. 10, where the angles θ and ϕ are defined in Fig. 7.

open ended and the distance d_4 between the feeding point of the last radiating element and the open end of the cable is $(3/4)\lambda_g$. Near the feeding point of the array, an impedance matching section is formed. The section consists of a quarter wavelength impedance transformer with a coaxial cable. The impedance matching is carried out as follows: by varying the distance d_0 between the feeding point of the array and that of the first radiating element (see Fig. 10) the imaginary part of $Z_{\rm in}$ can be canceled, where $Z_{\rm in}$ is calculated by (116). Now we have $Z_{\rm in} = Z_r = \text{real}$. The characteristic impedance Z_t of a quarter wavelength impedance transformer is determined by $Z_t = \sqrt{Z_r Z_f}$ to realize the matching, where Z_f is the characteristic impedance of the feeding coaxial cable. The designed parameters of the transformer are as follows: the inner and outer radii of the coaxial cable are $0.0026\lambda_{f0}$ and $0.010\lambda_{f0}$, respectively, the length of the coaxial cable is $(1/4)\lambda_{f0}$, where $\varepsilon_r = 1$ inside and $d_0 = 0.44\lambda_g$. Fig. 11 shows a comparison between calculated and measured values of the return loss of the fabricated array, where the input impedance was designed to be matched at f_0. The correspondence between the two values is considered to be fair, however, not negligible disagreements are observed, which is considered to be due to the following reasons. The mutual couplings are neglected between the radiating elements outside the feeding cable. The region near the open end of the feeding coaxial cable is simply modeled by the transmission line model in Fig. 10, some treatments, e.g., inclusion of radiation effects, may be needed. Finally, more precise modeling of the transition between the radiating element and the feeding coaxial cable is considered to be important to improve the correspondence in Fig. 11 as well as those in Fig. 6. Fig. 12 shows the radiation characteristics of the array. The efficiency—measured gain versus calculated directive gain—of the antenna was 91%. A good omnidirectional pattern in Az angles as well as a uniform aperture field illumination in El angles were observed.

VII. Summary

An electromagnetically coupled coaxial dipole array antenna has been proposed. An analysis as well as experimental verifications of the antenna have been carried out.

Appendix

In this Appendix, a factorization procedure for $L(\alpha)$ is described. First of all, we decompose $L(\alpha)$ into two functions $L^{(1)}(\alpha)$ and $L^{(2)}(\alpha)$ as follows:

$$\begin{aligned} L(\alpha) &= L^{(1)}(\alpha)L^{(2)}(\alpha) \\ L^{(1)}(\alpha) &= I_0(\gamma b)K_0(\gamma a) - K_0(\gamma b)I_0(\gamma a) \\ &= \frac{\pi}{2}\{J_0(\kappa a)N_0(\kappa b) - N_0(\kappa a)J_0(\kappa b)\} \\ L^{(2)}(\alpha) &= \frac{K_0(\gamma b)}{K_0(\gamma a)}. \end{aligned}$$

As the integral function $L^{(1)}(\alpha)$ is even with respect to α, the following factorization into the infinite product form is possible [8]–[11]:

$$\begin{aligned} L^{(1)}(\alpha) &= L_+^{(1)}(\alpha)L_-^{(1)}(\alpha) \\ L_+^{(1)}(\alpha) &= L_-^{(1)}(-\alpha) \\ &= \{L^{(1)}(0)\}^{1/2} e^{-\chi^{(1)}(\alpha)} \prod_{n=1}^{\infty} \left(1 + \frac{\alpha}{\alpha_n}\right)^{-\frac{\alpha(b-a)}{n\pi i}} \\ \chi^{(1)}(\alpha) &= \frac{\alpha(b-a)}{\pi i}\left[1 - C_e - \ln\left\{\frac{\alpha(b-a)}{\pi i}\right\}\right] \end{aligned}$$

where α_n is a zero point of $L^{(1)}(\alpha)$ in the upper-half α plane and it is located at $\alpha_n \sim n\pi i/(b-a)$ as $n \to \infty$. $\chi^{(1)}(\alpha)$ has been determined such that $L_+^{(1)}(\alpha)$ has an algebraic growth as $|\alpha| \to \infty$, $|\tau| < k_2$; in this case $L_+^{(1)}(\alpha) \sim \alpha^{-1/2}$. It can be also shown that $L_-^{(1)}(\alpha) \sim \alpha^{-1/2}$. For $L^{(2)}(\alpha)$, the Bates–Mittra factorization formula for $K_0(\gamma a)$ [9] is applied:

$$\begin{aligned} K_0(\gamma a) &= G(\alpha) \\ &= G_+(\alpha)G_-(\alpha) \\ G_+(\alpha) &= \left[\frac{\pi i}{2}H_0^{(1)}(ka)\right]^{1/2} \\ &\quad \times \exp\left\{-\frac{ika}{2} + \frac{ia\gamma}{\pi}\ln\left(\frac{\alpha-\gamma}{k}\right) + q(\alpha,a)\right\} \\ q(\alpha,a) &= \int_0^{\infty} f(\omega,\alpha,a)\,d\omega \\ f(\omega,\alpha,a) &= \frac{a}{\pi}\left[1 - \frac{2}{\pi\omega a}\cdot\frac{1}{\{J_0(\omega a)\}^2 + \{N_0(\omega a)\}^2}\right] \\ &\quad \times \ln\left(1 + \frac{\alpha}{\sqrt{k^2-\omega^2}}\right) \\ \sqrt{k^2-\omega^2} &= i\sqrt{\omega^2-k^2} \end{aligned}$$

$$G_+(\alpha) \sim \alpha^{-1/4} \exp\left\{ \frac{i\alpha a}{\pi} \ln\left(\frac{2\alpha}{k}\right)\right\} \quad (|\sigma| \to \infty, \tau > -k_2).$$

From the above formulas, $L^{(2)}(\alpha)$ is factorized as follows:

$$\begin{aligned} L^{(2)}(\alpha) &= L_+^{(2)}(\alpha) L_-^{(2)}(\alpha) \\ L_+^{(2)}(\alpha) &= L_-^{(2)}(-\alpha) \\ &= e^{-\chi^{(2)}(\alpha)} \left[\frac{H_0^{(1)}(kb)}{H_0^{(1)}(ka)}\right]^{1/2} \cdot \exp\left\{ -\frac{ik(b-a)}{2} \right. \\ &\quad \left. + \frac{i\gamma(b-a)}{\pi} \ln\left(\frac{\alpha-\gamma}{k}\right) + \xi(\alpha,a,b)\right\} \\ \xi(\alpha,a,b) &= q(\alpha,b) - q(\alpha,a) \\ \chi^{(2)}(\alpha) &= \frac{\alpha(b-a)}{\pi i} \ln\frac{2\alpha}{k} \end{aligned}$$

where $L_+^{(2)}(\alpha) \sim 1$ and $L_-^{(2)}(\alpha) \sim 1$ can be shown in $|\tau| < k_2$ as $|\alpha| \to \infty$.

Now we have $L_-(\alpha) = L_-^{(1)}(\alpha) L_-^{(2)}(\alpha) \sim \alpha^{-1/2}$ and $L_+(\alpha) = L_+^{(1)}(\alpha) L_+^{(2)}(\alpha) \sim \alpha^{-1/2}$, which prove (37).

ACKNOWLEDGMENT

The authors would like to thank Prof. K. Kobayashi of Chuo University, Tokyo, Japan, for his advice about applications of Wiener–Hopf techniques. They also would like to thank M. Murotani of Mitsubishi Electric Corporation, Tokyo, for his valuable comment on the development of approximate formulas in Section II.

REFERENCES

[1] H. A. Wheeler, "A vertical antenna made of transposed section of coaxial cable," *IRE Conv. Rec.*, vol. 4, pt. 1, pp. 160–164, 1956.

[2] T. J. Judasz, W. L. Ecklund, and B. B. Balsley, "The coaxial collinear antenna: Current distribution from the cylindrical antenna equation," *IEEE Trans. Antennas Propagat.*, vol. AP-35, pp. 327–331, Mar. 1987.

[3] T. J. Judasz and B. B. Balsley, "Improved theoretical and experimental models for the coaxial collinear antenna," *IEEE Trans. Antennas Propagat.*, vol. 37, pp. 289–296, Mar. 1989.

[4] A. Sakitani and S. Egashira, "Analysis of coaxial collinear antenna: Recurrence formula of voltages and admittances at connections," *IEEE Trans. Antennas Propagat.*, vol. 39, pp. 15–20, Jan. 1991.

[5] M. Ono, T. Numazaki, and M. Mizusawa, "A high-gain omnidirectional antenna made of a printed element," *Trans. IECE*, vol. 63-B, no. 1, pp. 25–31, 1980 (Japan).

[6] P. Volta, "Design and development of an omnidirectional antenna with a collinear array of slots," *Microwave J.*, vol. 25, no. 12, pp. 111–115, 1982.

[7] K. Cho, T. Hori, H. Tozawa, and S. Kiya, "Bidirectional collinear antenna with arc parasitic plates," in *IEEE AP-S Int. Symp. Dig.*, 1995, pp. 1414–1417.

[8] B. Noble, *Methods Based on the Wiener–Hopf Technique*. New York: Chelsea, 1988.

[9] R. Mittra and S. W. Lee, *Analytical Techniques in the Theory of Guided Waves*. New York: Macmillan, 1971.

[10] K. Kobayashi, "Wiener-Hopf and modified residue calculus techniques," in *Analysis Methods for Electromagnetic Wave Problems*, E. Yamashita, Ed. Norwood, MA: Artech House, 1990, ch. 8.

[11] K. Kobayashi, "The Wiener–Hopf technique with applications to scattering and diffraction problems," in *A Course of Applied Mathematics*, K. Horiuchi,Ed. Tokyo, Japan: Corona, 1989, ch. 9 (in Japanese).

[12] N. Marcuvitz, *Waveguide Handbook*. London, U.K.: Peter Peregrinus, 1986, sec. 4–15, pp. 208–213.

[13] T. T. Wu, "Input admittance of infinitely long dipole antennas driven from coaxial lines," *J. Math. Phys.*, vol. 3, no. 6, pp. 1298–1301, 1962.

[14] T. S. Bird, "Exact solution of open-ended coaxial waveguide with centre conductor of infinite extent and applications," *Proc. Inst. Elect. Eng.*, vol. 134, pt. H, no. 5, pp. 443–448, Oct. 1987.

[15] Y. M. Chen and J. B. Keller, "Current on and input impedance of a cylindrical antenna," *J. Res. Nat. Bur. Stand.*, vol. 66D, no. 1, pp. 15–21, 1962.

[16] S. W. Lee and R. Mittra, "Admittance of a solid cylindrical antenna," *Can. J. Phys.*, vol. 47, pp. 1959–1970, 1969.

[17] J. R. Wait, *Electromagnetic Radiation from Cylindrical Structures*. London, U.K.: Peter Peregrinus, sec. 4, 1988.

[18] H. Jasik, Ed., *Antenna Engineering Handbook*. New York: McGraw-Hill, 1961, ch. 9.

[19] R. E. Collin, *Antenna Theory*. New York: McGraw-Hill, 1969, ch. 14, pt. 1, p. 590.

Hiroaki Miyashita (M'90) was born in Shimoda, Shizuoka, Japan, on May 2, 1964. He received the B.S. degree in applied physics from the University of Tokyo, Japan, in 1987. He is currently working toward the Ph.D. degree at the Radio Atmospheric Science Center, Kyoto University, Kyoto, Japan.

He is currently with Kamakura Works, Mitsubishi Electric Corporation, Tokyo, Japan. He is also with Radio Atmospheric Science Center, Kyoto University, Kyoto, Japan. His primary research activities are in antenna analysis and applied mathematics for wave phenomena.

Mr. Miyashita received IEEE Antennas and Propagation Society Tokyo Chapter Young Engineer Award in 1994 and the 1995 Young Engineer Award of IEICE Japan. He is a member of the IEICE, Japan, the American Physical Society, and the American Mathematical Society.

Hiroyuki Ohmine (M'92) was born in Kitami, Hokkaido, Japan, on August 14, 1961. He received the B.E. degree from Kitami Institute of Technology, Kitami, Japan, in 1984, and the M.E. and D.E. degrees from Hokkaido University, Sapporo, Japan, in 1986 and 1997, respectively.

He joined Mitsubishi Electric Corporation, Tokyo, Japan, in 1986. Since then he has been engaged in the research and development of millimeter-wave and microwave antennas for mobile communication systems and radar systems. He is currently with the Antenna Department of Information Technology R&D Center, there.

Dr. Ohmine is a member of the IEICE Japan.

Kazushi Nishizawa (M'94) was born in Koshigaya, Saitama, Japan, on September 25, 1968. He received the B.E. degree in electrical engineering from Tohoku University, Sendai, Japan, in 1992.

He joined Mitsubishi Electric Corporation, Tokyo, Japan, in 1992, and has been engaged in the research and development on antennas for radar systems and satellite communications systems. He is currently with the Antenna Department of Information Technology R&D Center there.

Mr. Nishizawa received the IEEE Antennas and Propagation Society Tokyo Chapter Young Engineer Award in 1997. He is a member of the IEICE Japan.

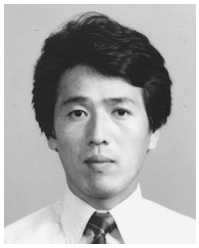

Shigeru Makino (M'90–SM'95) was born in Fukuyama, Hiroshima, Japan, on October 16, 1954. He received the B.E. and Ph.D. degrees in electrical engineering from Kyoto University, Kyoto, Japan, in 1977 and 1994, respectively.

He joined Mitsubishi Electric Corporation, Tokyo, Japan, in 1977 and has been engaged in research on antennas for public communications and satellite communications. He is currently the Team Leader of Antenna Department of Information Technology R&D Center there.

Dr. Makino is a member of the IEICE Japan.

Shuji Urasaki (M'85–SM'95) received the B.S., M.S., and Ph.D. degrees all in electronic engineering, Hokkaido University, Sapporo, Japan, in 1967, 1969, and 1985, respectively.

In 1969, he joined Mitsubishi Electric Corporation, Tokyo, Japan. Since then he has worked on antennas for public communications, satellite communications, and radar systems. Currently, he is the General Manager of Electro-Optics & Microwave Systems Laboratory of Information Technology R&D Center, Mitsubishi.

Dr. Urasaki is a member of IEICE Japan.